Journal of the European Ceramic Society 39 (2019) 3484–3490

Contents lists available at ScienceDirect

Journal of the European Ceramic Society

journal homepage: www.elsevier.com/locate/jeurceramsoc

Original Article

Micrograded ceramic-metal composites

Thomaz Augusto Guisard Restivo[a,b,c,*], Rafael Fonseca Beccari[a], Wellington Rafael Padilha[a], Michelangelo Durazzo[b], Victor Bridi Telles[c], Jorge Coleti[c], Chieko Yamagata[b], Antonio Carlos da Silva[b], Eduardo Suzuki[a], Jorge Alberto Soares Tenório[c], Sonia Regina Homem Mello-Castanho[b]

[a] University of Sorocaba – UNISO, Brazil
[b] Nuclear and Energetic Research Institute – IPEN, Brazil
[c] Polytechnics of Sao Paulo – EPUSP, Brazil

ARTICLE INFO

Keywords:
Cermet
Graded ceramic
Radiation shield
Thermal insulation material
Emissivity

ABSTRACT

The article shows new designed cermets and processes concerning primary to applications as thermal insulation materials with low emissivity. A new projected microstructure was obtained where dense regions (micropellets) rest inside the main porous pellet. The feature resembles a frozen hypercube, therefore such architecture is called hyper-pellet/ cermet. The processing method to obtain the hyper-cermet is based on sequential tape castings and sintering techniques. Ni-zirconia lamellae were prepared by a special mechanochemical process followed by sintering, which remain inside the main pellets as a dense region. The whole pellet is turned to be porous by employing pore-forming additives. All the constituents and porosity shapes are aligned along the disc/ flake planes. Thermal conductivity is estimated for the materials up to 800 °C by a flash diffusivimeter. Ceramographic analyses show graded density regions with directional constituents and pores. Applications of such materials are foreseen as temperature insulation materials and thermal radiation shields.

1. Introduction

Ceramic-metal composites materials (cermets) have been considered for numerous applications due to their properties, once they can feature combining properties like metal toughness and conductivity with strong hardness and high stability of ceramics [1]. This is the case at several traditional products, like cement carbide tools and dies. The electrochemical and surface reaction activity of metals such as Ni and Cu give rise to the development of a vast sort of catalysts presently used at chemical and energy generation plants.

The present paper deals with a new application for cermet materials: thermal insulation of heated devices where radiation heat transfer flow is concerned or dominates. Generally, ceramic materials show rather low thermal conductivities and good refractoriness, being a good choice when an insulation material is required for high temperature. However, most part of ceramic types is translucent to infrared radiation emitted from heated bodies at, say, 1000 °C. This fact effects negatively their performance with respect to the reduction of the outside temperature of an internally heated device or heat source to be thermal insulated from the environment. Heat losses and low temperature profiles impact energy efficient at several processes, like heated tubes, reactors and gas processing/ burning systems.

Radiation shield materials have been used to insulate high temperature reactors, combustion devices and furnaces [2,3]. Most of them is composed by overlapping several parallel metal sheet interposed by ceramic low conductivity inserts.

The classical formulation [3,4] considers 2 large parallel plates with surface area A at temperatures T_1 and T_2 where the rate of radiation heat transfer between such surfaces is given by:

$$Q_{12} = \frac{A\sigma(T_1^4 - T_2^4)}{\frac{1}{\varepsilon} + \frac{1}{\varepsilon} - 1} \quad (1)$$

Eq. (1) is valid if the emissivities ε of all surfaces are equal and the view factor F_{12} is unity. Introducing some radiation shield plates assigned from 3 to N, the equation results:

$$Q_{12,N} = \frac{A\sigma(T_1^4 - T_2^4)}{\left(\frac{1}{\varepsilon} + \frac{1}{\varepsilon} - 1\right) + \left(\frac{1}{\varepsilon} + \frac{1}{\varepsilon} - 1\right)_3 + \left(\frac{1}{\varepsilon} + \frac{1}{\varepsilon} - 1\right)_4 + \ldots + \left(\frac{1}{\varepsilon} + \frac{1}{\varepsilon} - 1\right)_N} = \frac{A\sigma(T_1^4 - T_2^4)}{(N+1)\left(\frac{1}{\varepsilon} + \frac{1}{\varepsilon} - 1\right)} \quad (2)$$

* Corresponding author at: University of Sorocaba – UNISO, Rod. Raposo Tavares km 92, 18023000 Sorocaba SP, Brazil.
E-mail addresses: thomaz@protolab.com.br, restivo@protolab.com.br (T.A. Guisard Restivo).

https://doi.org/10.1016/j.jeurceramsoc.2019.03.018
Received 13 November 2018; Received in revised form 5 March 2019; Accepted 8 March 2019
Available online 09 March 2019
0955-2219/ © 2019 Elsevier Ltd. All rights reserved.

Therefore, the ratio between the rates of radiation heat transfer from the plates without shields to N shields is N + 1, say the heat transfer rate is reduced by this amount. Also, opaque materials of small emissivity are more efficient on reducing the heat transfer rate, since the sum $\alpha + \rho = 1$ (absorptivity + reflectivity) and for thermal equilibrium $\alpha = \varepsilon$. Thus, low emissivity imply at high reflectivity, which is found in bright metallic surfaces.

Radiation shields are macro-devices. By analogy, micro-devices have potential application, being dealt in this work. The authors have proposed a new approach in order to improve the insulation materials used at hot systems: incorporate dispersed and oriented metal lamellae, or micro-plates, embedded in a ceramic matrix. The design foresees several metal lamellae acting as micro-radiation shields. However, most metal sheets can undergo oxidation at high temperatures leading to reflectance dropping. Therefore, it is needed to protect the metal surfaces from air oxidation. The material design solution is found by encapsulating the lamellae into dense ceramic layers. Such metal-containing regions acts as inner dense flat pellets surrounded by an outer porous ceramic pellet in order to reach low global thermal conductivity simultaneously. In this regard, a cermet with projected microstructure is designed which features resembling a flat hypercube. Although the analogy is merely based on drawn images [5], it carries out more meaningfulness in the sense the hypercube can be seen as an inner cube inside another cube that was expanded from the former. Thus, considering now the dense inner pellet as described above (for protecting embedded metal against oxidation), it will generate a less dense pellet or a porous one (outer pellet) when expanded. Fig. 1 shows such inspiring design development to embedded cermet material, where the hypercube drawings represent the 3-D projection of a 4-D cube. Other feature of such material design relates to the pore structure, which is composed of thin flattened oriented pores, leading to further reduction of the bulk thermal conductivity. The material project foresees to stack several dense, metal-containing ceramic flakes, through the pellet thickness, with careful controlled sizes, to play the role of a micro radiation shield. In the face of such considerations, the new material is named as micrograded cermet, or even “hyper-ceramic (cermet)”. The material design is outlined in Fig. 2 at two possible forms: disk and flake powder. It can be seen at the cross-section drawings shown in Fig. 3 the embedded metal micro-plates at dense regions which are superimposed inside the bodies, while several parts are also stacked for potentializing the radiation shield effect. Some photon reflections are schematized in the figure, suggesting there is a strong reduction on the rate of radiation heat transfer (represented by arrows). Conducting phonons are expected to be extinguished at flat pore interfaces, perpendicular to heat flow, once there are no paths to proceed by scattering/ recombination.

Insulation materials often contain radiation shields like metal plates and ceramic boards, including opacifiers such as TiO_2 and low density fumed silica, which scatter the radiation, as well as some absorbing materials like carbon soot [6,7]. The highest insulating materials are known as Vacuum Insulation Panels (VIP) and Nano Insulation Materials (NIM), reaching apparent thermal conductivity smaller than 0.02 W/mK at ambient temperature and normal pressure. These materials show very low densities below 0.02 kg/m^3, whereas finding application at near ambient or sub-zero temperatures. Such evacuated panels or foils have metal sheets layers with fibrous polymers, foams, powders or glass wood. However, vacuum leaks can lead to degradation of their performance with time. In the case of high temperature insulation materials, Multi-layer Thermal Insulation (MTI) has been investigated [8] consisting of metal coated reflective ceramic layers or screens with low emissivity, separated by spacers and shaped as a sandwich. The thermal conductivity can result as low as 0.1 W/mK at 800 °C due to reduction of the radiative heat transfer by the shields.

The main innovation of the present work is to obtain materials with a projected structure morphology containing layers of low emissivity – metal micro-plates or lamellae - enclosed in low conductivity ceramic with directional properties. In addition, such material is prepared in bulk form and can be self-settled during the application in a hot device as a powder, by fluidization, or even dispersed in paints. The hyper-cermet design will therefore reduce the radiation heat transfer and apparent thermal conductivity at high temperatures, leading to more efficient systems and energy savings.

2. Materials and methods

In other to fabricate the hyper-cermet material, an especial process method was developed. Metal powder was deformed into thin lamellae by high energy milling. The orientation of all flat constituents, including flake ceramic with metal lamellae and flat pores, was provided by tape casting-like methods due to doctor blade action. The pore structure was obtained by flaked pore-forming additives, which are gasified during pre-sintering treatments. In spite of a rather complex preparation method with several crossing steps, the unit processes are simple.

The starting materials employed for the preparation of the micrograded cermets were Ni powder 38 μm mean particle size (CIRQ Cromato) and a tetragonal zirconia 3 mols% yttria from Tosoh Co (YTZ), 40 nm particle size and BET = 16 m^2/g. YTZ ceramic is expected to full sinter at 1300 °C, or at least to close the pores with final density over 92%TD (theoretical density). High energy milling (mechanical alloying – MA) of Ni powder was performed in a shaker mill at 19 Hz frequency during 20 min, into hard steel vials and spheres. The ball to powder ratio was set at 5:1. Some YTZ powder was added at the end of the milling period. From such metal and zirconia powders, a processing sequence started: slurry preparation and tape casting, based on literature for YTZ slurries [9–11], as well as sintering steps. The whole process sequence and details are shown as a flowsheet in Fig. 4. Hyper-cermet is composed by INNER dense Ni-bearing zirconia (encapsulated) layers plus the OUTER zirconia porous material, composing a final micrograded hyper-cermet. The nominal composition was set at 15 vol. % Ni – YTZ, mainly concentrated in the core portion. Oriented pores were obtained by adding pore-forming (flaky plate powder graphite Dinamica < 50 μm) which is burned during the oxidative sintering period. Disk samples were prepared through a new developed tape casting method - *tape-moulding casting* - carrying out the tape casting

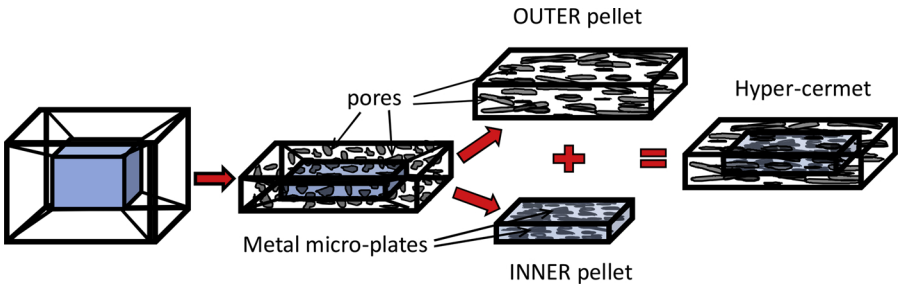

Fig. 1. 3-D Hyper-cube projection (perspective drawing) deformed to flattened hyper-pellet composed by an outer porous ceramic pellet and an inner dense pellet containing encapsulated metal micro-plates; the hyper-cermet is the final developed design with aligned pores and metal lamellae.

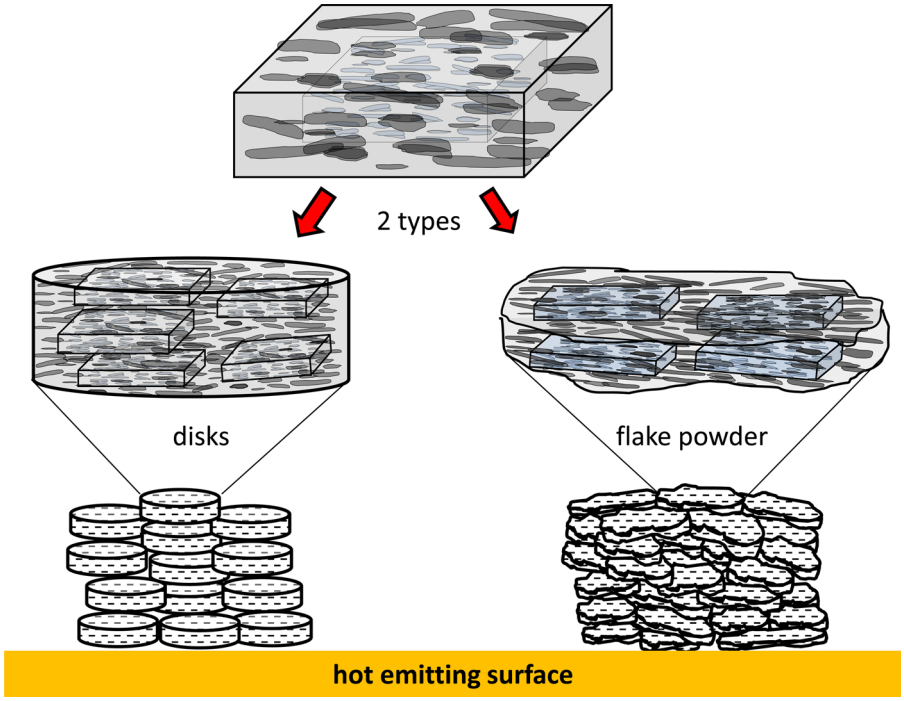

Fig. 2. Two hyper-cermet products: disks and flake powder; cermet bodies can be stacked to multiply the heat radiation shield effect and thermal insulation of a hot surface.

over a perforated plate mould with thousands of 4-mm holes. The disks so casted and dried were withdrawn from the holes even naturally or by punch actions. Other product version - flake powder - was obtained by granulating the plain tape before the final sintering. In both cases, fine powder below 45 μm was withdrawn from the test samples.

Tape casted and sintered materials were characterized through thermal analysis experiments coupled to mass spectrometer (TG/DTA-MS). Ceramographic specimens were prepared by vacuum impregnation and observed at optical microscope and SEM for revealing the microstructure features. Thermal conductivity was evaluated from a flash diffusivimeter apparatus (ASTM E1461-13) employing a powder sample holder, using the thermal quadrupole analytical method inbuilt at specific softwares [13,14]. Eqs. (3)–(6) encompass the thermophysical properties of materials and stainless steel sample holder, measured quantities and thermal diffusivity from the diffusivimeter, allowing to determine the thermal conductivity K of a powder or disk sample of thickness e from ambient to 800 °C.

$$K = \frac{e}{\frac{e_T}{K_{eff}} + \frac{e_{ss}}{K_{ss}}}, \tag{3}$$

$$K_{eff} = \propto_{eff} . \rho_{eff} . C_{peff}, \tag{4}$$

$$C_{peff} = \frac{\rho_{ss} . C_{pss} . e_{ss} + \rho . C_p . e}{\rho_{ss} . e_{ss} + \rho . e}, \tag{5}$$

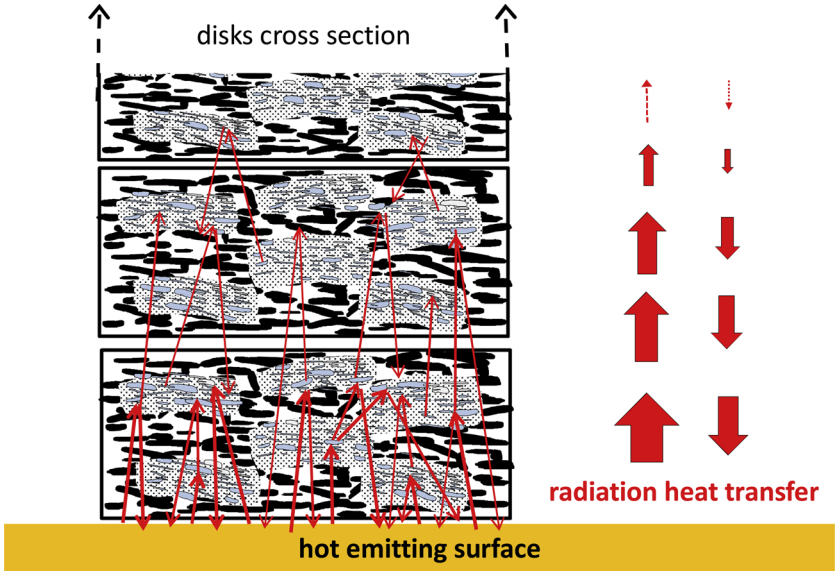

Fig. 3. Stacked disks schematic cross-section showing dense regions with metal thin lamellae; some photon reflections illustrate the reduction of the rate of radiation heat transfer for insulation.

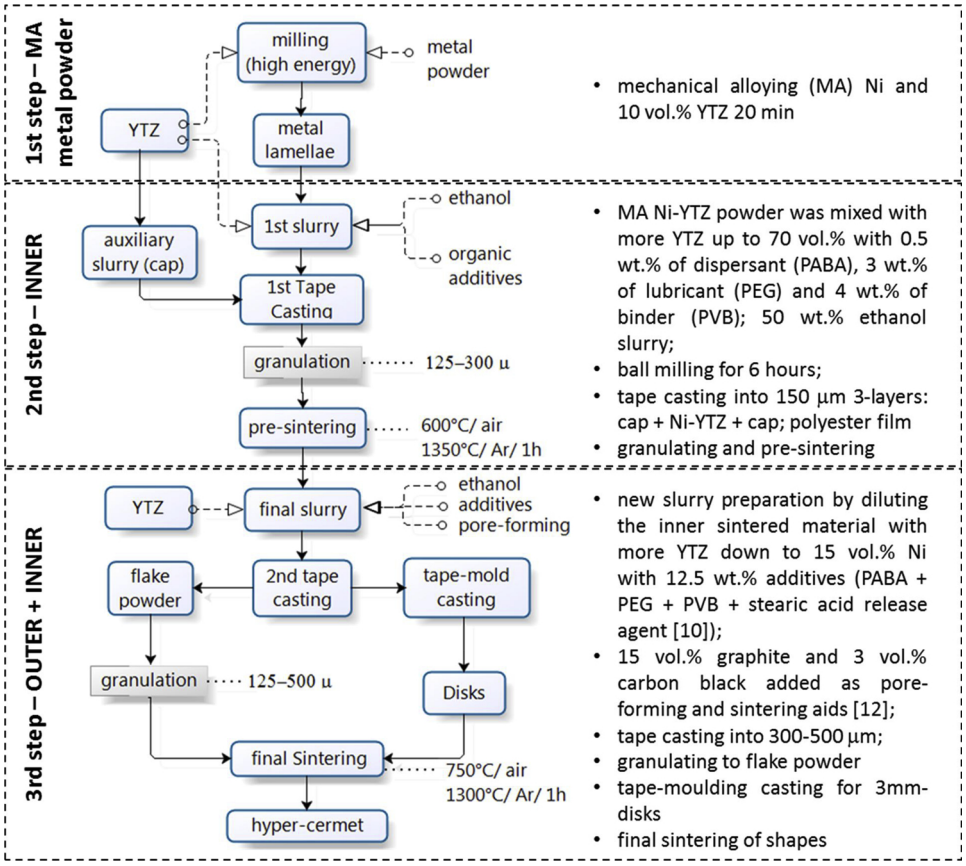

Fig. 4. Hyper-cermet process flowsheet and some details of composition and methods at each step [12].

$$\rho_{eff} = \frac{\rho_{ss}.\ e_{ss} + \rho.\ e}{e_{ss} + e}, \quad (6)$$

where α, Cp and ρ are the material thermal diffusivity, heat capacity and density; eff subscripts refer to effective properties, ss subscript relates to stainless steel sample holder, e_T to sample holder total thickness and $\propto_{eff}$ is equal to the measured diffusivity. The cermet and holder materials Cp and coefficient of thermal expansion were taken from literature [15–17]. Disk, flake powder and silica-alumina blanket samples were also evaluated regarding to the thermal conductivity at a Ctherm TCi analyser at 20 °C (ASTM D7984-16).

3. Results and discussion

Themogravimetry and mass spectrometry (MS) of green flake powder under air/N_2 flow is shown in Fig. 5. Mass losses are linked to CO_2 release and O_2 consumption. Based on such signals and TG curve, the first mass losses up to about 500 °C are related to binder and additives decomposition and oxidation followed by the oxidation of pore-forming agents at higher temperatures from 600 to 1000 °C. After 940 °C, Ni starts to oxidize. Therefore, to maintain Ni in the metallic state, the atmosphere must be changed to an inert gas (argon). Accordingly, heating steps under air are limited to 750 °C, as pointed out in Fig. 4.

Fig. 6 shows the materials processing sequence: Ni powder round particles deformation into lamellae by MA, which was added to zirconia for tape casting; granulating and pre-sintering; tape (-moulding) casting a second slurry with pore-forming additives and sintering flakes and disks cermets. It can be noted the pre-sintered material has layered structure due to 3 successive tape castings, where bottom and top YTZ caps the inner Ni-YTZ layer. The final powder displays some Ni bright

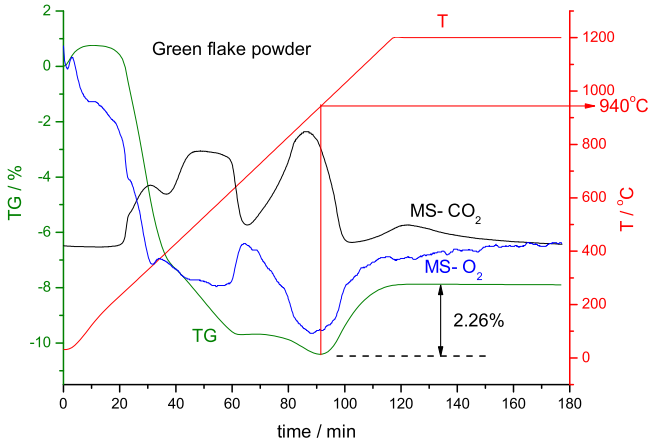

Fig. 5. Green flake powder thermogram coupled to mass spectrometer; heating rate 10 °C/min under air/ N_2 (20/20 ml/min); the weight gain for Ni oxidation is corrected to comply with the solid content.

points whereas most part is encapsulated by zirconia. The sintered as-prepared materials – disks and flake powder microstructure - are shown in Fig. 7. The disks shape is somewhat convex due to the slurry meniscus formation at tape-moulding casting. One can note at the powder microstructure the bright Ni layers encapsulated by zirconia like a sandwich at some points, whereas it is totally embedded in others. These features will increase the oxidation resistance of metal platelets.

Table 1 compiles some physical characteristics of the materials. The calculated theoretical density was 653 g/cm^3 for a nominal content of 15 vol.% (20.7 wt.% Ni) in YTZ. Tap densities are low, especially for

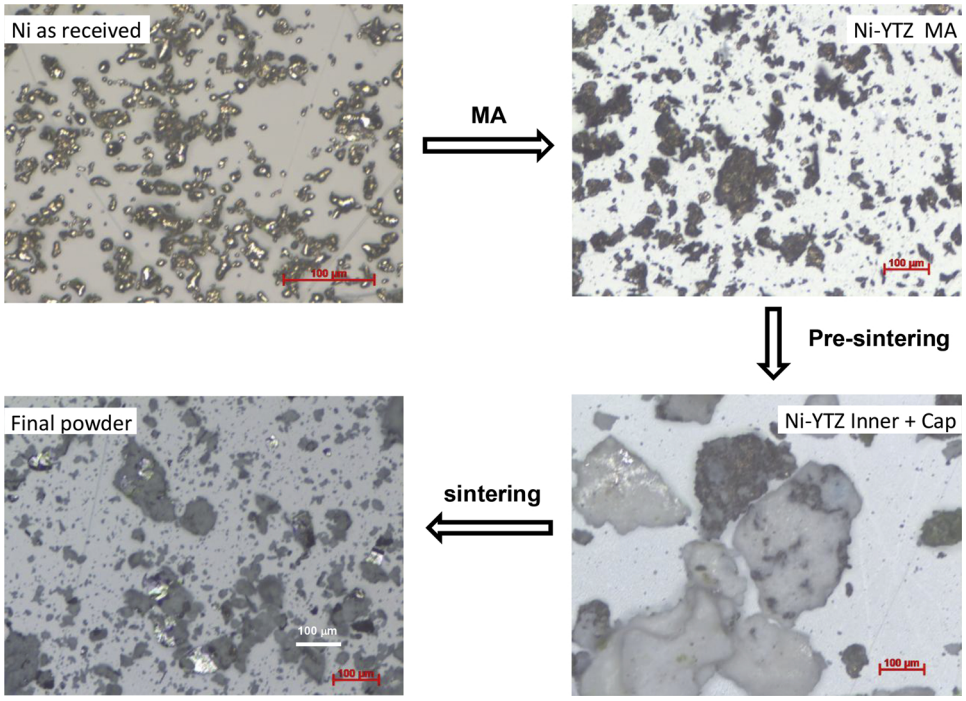

Fig. 6. Microstructure of tape/ granulated powder according to the processing sequence: mechanical alloyed Ni powder, tape casting of encapsulated Ni into YTZ followed by pre-sintering; second tape-casting and final sintering.

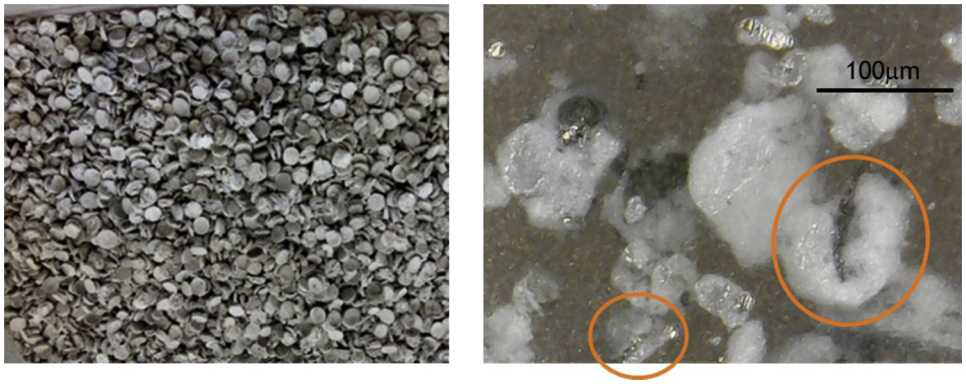

Fig. 7. Aspects of 3-mm disks and flake powder morphology showing encapsulated Ni platelets into zirconia (emphasis on sandwich type cermet).

disks, while the densities measured at a pycnometer approach the theoretical value. In this case, the coarse flake powder, retained at 125 µm sieve and, to a lesser extent, the moulded disks, have rather small values suggesting there are some closed pores inside the particles or bodies.

Elongated big pores can be seen in Fig. 8 to be aligned to the disk surface, as well as Ni lamellae. The SEM-BSE images show little contrast difference between Ni and YTZ, where they can be distinguished since the metal is bulk while zirconia presents several small closed pores inside. It can be also noted that Ni is surrounded either by zirconia or big pores from burned pore-forming additives. This feature would help to avoid oxygen for metal oxidation, in spite of the large and elongated pores are supposed to have an open structure. It is also observed a small graphite plate not burned during oxidative sintering steps. The optical images confirm the alignment of bright Ni lamellae, most of them parallel to disk surface, but less evident for flake powders. EDS measurements at several regions varied from 14.9 to 15.7 wt.% Ni. Such results suggest the Ni content is somewhat smaller than the nominal one, besides the occurrence of Ni pulling out during polishing and settling of heavier Ni-bearing particles.

The thermal behaviour of these materials after final sintering is shown in Fig. 9. Thermogravimetric and MS curves up to 1100 °C allow verifying the flake powder material is rather more resistant to Ni oxidation than the disk one. The former has smaller weight gain and the

Table 1
Physical characterization of disks and flake powders; disks: geometrical density; calculated theoretical density %TD = 653 g/cm^3.

Material	Mass g	Density g/cm^3	%TD	Tap density g/cm^3/%TD	Pycnometry g/cm^3
Disks	0.007–0.026	2.48–3.16	38.8–49.5	1.15/17.6	6.47
Flake coarse				1.52/23.3	6.39
Flake coarse + fine				2.33/35.7	6.52

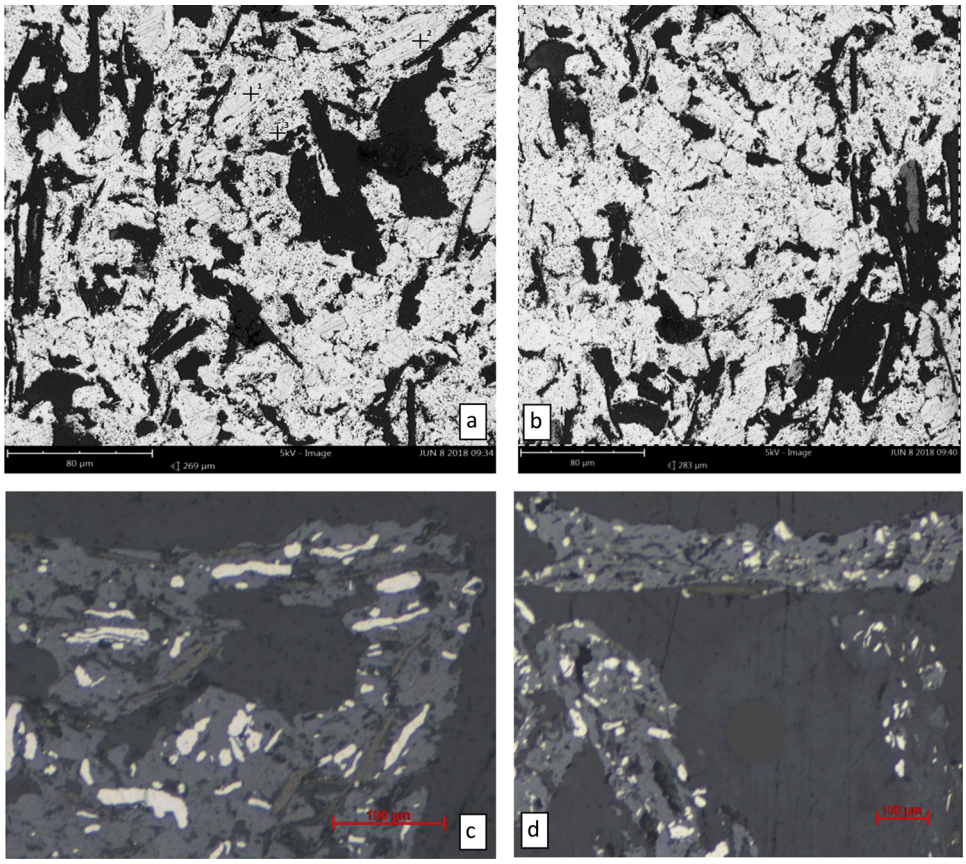

Fig. 8. (a) SEM-BSE images of disk sample (vertical disk plane): Ni is distinguish by crosses surrounded by zirconia with thin closed pores; (b) grey platelet is some remaining graphite not totally burned; (c, d) optical microscopy of disk corner and flake powder, showing aligned constituents (For interpretation of the references to colour in this figure legend, the reader is referred to the web version of this article).

oxidation onset temperature is higher. The nominal weight gain of Ni oxidation to NiO is 3.21% for 15 wt.% Ni content at the materials. The difference indicates there remains some encapsulated metal into zirconia, which protects it from oxidation up to 1100 °C. It seems the tape-moulding casting process and sintering during disks preparation has somehow exposed more Ni to oxygen due to cracking or too fast gas releasing from binder/ pore-forming burning at oxidative steps. Anyway, the process is delicate regarding heating rates and atmospheres.

Fig. 10 shows a plot of the thermal conductivity measurements at flash diffusivimeter from stainless steel sample holder of disk sample. The Ni content was set at 15 wt.% for density and C_p calculations. It is interesting to note the values increase up to 500 °C, afterward decreasing at higher temperatures. Actually, the measured thermal diffusivity/ conductivity is apparent in the sense it comprises both conduction and radiation heat transfer phenomena. The material design argue the radiation heat flow would be reduced by reflections at embedded Ni lamellae due to radiation shield effect, which is more pronounced at high temperature. The results suggest the material behaves as predicted where the total apparent thermal conductivity decreasing at high temperature.

Thermal conductivity values measured from 20 °C up to 800 °C are shown in Table 2 compared to some high temperature insulation materials data from literature [6,7,18,20]. The TCi method results are smaller when compared to flash instrument. This fact can be explained since the powder and disks are loosed placed over the TCi sensor

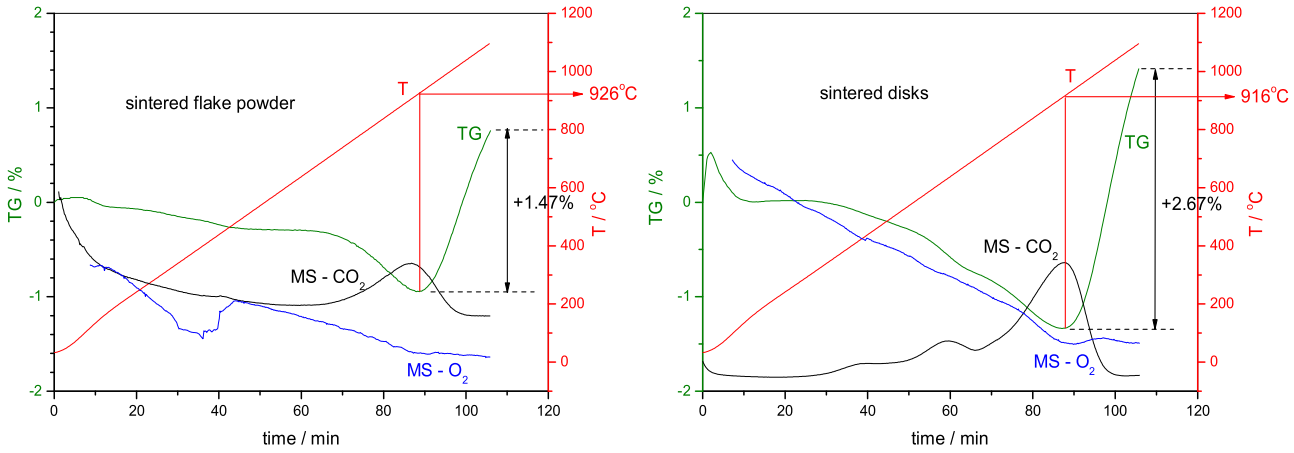

Fig. 9. Thermogravimetry coupled to MS of final prepared flake powder and disks; heating rate 10oC/min under air/ N_2 (20/20 ml/min); the weight gain for Ni oxidation is corrected to comply with solid content. The theoretical weight gain for oxidation from Ni to NiO is 3.21 wt.%.

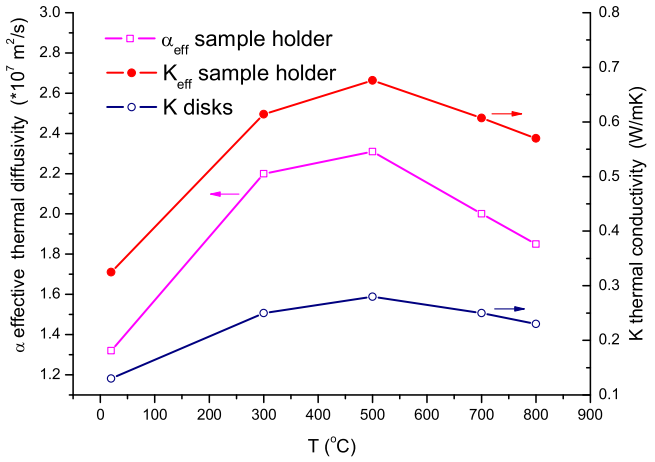

Fig. 10. Effective (measured) thermal diffusivity and conductivity of charged sample holder and the resulted thermal conductivity of hyper-cermet disks; uncertainty 5.13% [19].

Table 2
Apparent thermal conductivity comparison of some high temperature insulating materials [6,7,18,20] with measured hyper-cermet samples at present work; methods: CTi (ASTM D7984-16) and flash (ASTM E1461-13).

Insulation material	Density (kg/m^3)	K_{therm} (W/mK)	T points (°C)
High alumina fiber blanket	128	0.04–0.20	165–864
Silica + glass fiber + TiO_2	~100	0.025–0.029	300–700
Carbon aerogel	80–275	0.015–0.12	25
High T VIP Carbon felt - Silica	156	1.26–3.24–1.84	25–500–1200
ZrO_2 powder (METCO 6700)	842	0.311	80
Silica-alumina blanket (CTi)	128	0.041 ± 0.0001	25
flake powder (CTi)	loose packed	0.0507 ± 0.0001	25
disks (CTi)	loose packed	0.0697 ± 0.0001	25
disks (flash)	1040	0.13–0.28–0.23	25–500–800
YTZ cap (flash)	1672	0.320–0,327	25–100

Flash method measurements uncertainty: 5.13% [19].

without compaction. Conversely, in flash instrument, the sample holder is threaded for pressing and contacting the material on the inner chamber surfaces. Thermophysical properties, as expected, are very sensitive to porosity and void spaces thoroughly the material. The comparison with a commercial silica-alumina blanket (128 kg/m^3) demonstrates the thermal conductivity of the hyper-cermet is close to actual high insulation products. The presently developed material has comparable low values of thermal conductivity, but with much higher density. For instance, the density of the new material is 10 times greater than the alumina blanket. Contrasting to the developed materials, blankets are rather transparent to thermal radiation. Moreover, when comparing the measurements of cermet flake powder or disks with pure YTZ tape casted (cap – auxiliary slurry), which has been granulated and sieved as the final flake powder, it can be realised the cermet materials have considerable lower thermal conductivity. (similar result is included at Table 2 for YSZ powder [20]). This fact gives more support to the development of the hyper-cermet as conceived in the present article. It can be realised the hyper-cermet material has great potential, since the composition, porosity and material compaction during charge application can be adjusted to find high performance. The tap or disk density can be reduced by lowering the sintering temperature or increasing pore-forming amounts to find even smaller thermal conductivities. Theoretically, the metal content can be increased up to 30 vol.%, below the electrical percolation limit of the cermet, which means more parallel metallic lamellae for shielding. Other advantage is its refractoriness, leading to elevated thermal resistance to degradation and oxidation, rarely found in other insulating materials.

4. Conclusions

Projected cermet material with micrograded constituents, called hyper-cermet, was successfully prepared by an special process which the main features are the Ni-containing inner regions in lamellar form surrounded by porous ceramic, which rest aligned to the tape casting plane. These features can reduce both the thermal conductivity and radiation heat flow, the last by the radiation shielding effect taking place at stacked Ni lamellae. Inner regions are rather dense in order to protect the metal against air oxidation. The material can be employed at ambient conditions up to 1000 °C without strong degradation. The main concerns of the new process are: reduce metal settling from slurries, closing the pores at inner regions for protecting the metal flakes and the intermediate calcination in air atmosphere for burning out the pore-forming additives.

Thermal diffusivity/ conductivity measurements have shown the material is more insulating at high temperatures, when radiative heat flow becomes more important, indicating the validity of such material design. Heat savings are similar on comparing with silica-alumina blankets, which is about 10 times less dense than the present material and rather transparent to radiation.

Aknowledgements

The authors acknowledge CNPq Research Council proc. PDS - 150672/2012-8, Brazil and UNISO proc. IC - 100/2017, Brazil funds for scientific initiation fellowships.

References

[1] C. Woodford (2009/2017) Cermets, Retrieved from https://www.explainthatstuff.com/cermets.html (Accessed 10 november 2018).
[2] Kirk-Othmer, 5th ed., Encyclopedia of Chemical Technology vol. 12, Furnaces, Electric, Wiley, 2007.
[3] Y.A. Cengel, A.J. Ghajar, Heat and Mass Transfer: Fundamentals and Applications, 5th ed., McGraw-Hill, 2014.
[4] F.P. Incropera, Fundamentals of Heat and Mass Transfer, 7th ed., Wiley, 2007, p. 886.
[5] B. Polster, A Geometrical Picture Book, Springer-Verlag, New York, 1998, p. 291.
[6] A. Berge, P.är Johansson, Literature Review of High Performance Thermal Insulation, Report 2012:2, Chalmers University of Technology, 2012.
[7] J. Fricke, U. Heinemann, H.P. Ebert, Vacuum 82 (2008) 680–690.
[8] M. Tychanicz-Kwiecień, J. Wilk, P. Gil, J. Thermophys. Heat Transf. 33 (1) (2019) 271–284.
[9] D. Hotza, Review article: tape casting, Ceramica 43 (283–284) (1997) 157–164.
[10] D.J. Shanefield, Organic Additives and Ceramic Processing, Springer Science +Business Media, New York, 1995 311 p.
[11] H. Wang, Z. Gao, S.A. Barnett, Anode-supported solid oxide fuel cells fabricated by single step reduced-temperature co-firing, J. Electrochem. Soc. 163 (3) (2016) F196–F201.
[12] T.A.G. Restivo, M. Durazzo, S.R.H. Mello-Castanho, A.C. Moreira, S. Graciano, V.B. Telles, J.A.S. Tenorio, Low-temperature densification of ceramics and cermets by the intermediary stage activated sintering method, J. Therm. Anal. Calorim. 131 (2018) 249–258.
[13] T.A. Guisard-Restivo, Desenvolvimento de instrumento para a medida de difusividade térmica de materiais pelo método flash, Proceedings of the 47th Annual Meeting of the Brazilian Ceramic Society (2003) (Accessed 10 November 2018, http://www.protolab.com.br/Medir_difusividade.pdf.
[14] D. Maillet, S. André, J.C. Batsale, A. Degiovanni, C. Moyne, Thermal Quadrupoles: Solving the Heat Equation Through Integral Transforms, Wiley, 2000, p. 388p.
[15] M.W. Chase Jr, NIST-JANAF themochemical tables, fourth edition, J. Phys. Chem. Ref. Data Monogr. 9 (1998) 1–1951.
[16] B.M. Caruta, New Developments in Material Science Research, Nova Science Publ., 2007, p. p110.
[17] R.H. Bogaard, Thermal conductivity of selected stainless steel, in: T. Ashworth, D.R. Smith (Eds.), Thermal Conductivity 18. P.175, Plenun Press, 1985763 p.
[18] Y. Wang, et al., Preparation and characterization of new-type high-temperature vacuum insulation composites with graphite felt core material, Mater. Des. 99 (2016) 369–377.
[19] T.A.G. Restivo, Desenvolvimento de Instrumento para a Medida de Difusividade Térmica de Materiais pelo Método do Pulso de Energia – Fase II. 3rd. Report, process 01/08406, FAPESP, 2008, p. 18 (Accessed 2 March 2019), https://www.researchgate.net/publication/331473685_Developing_report_with_images_measurements_calculations_and_uncertainties.
[20] M. Drajewicza, K. Dychtoń, M. Góral, Thermal properties of YSZ powders for plasma spraying, Solid State Phenom. 227 (2015) 413–416.